The Aligarh Bulletin of Mathematics
Volume 44, Number 1 (2025), 1 - 28
ISSN: 0304-9787

Dynamical system techniques for stability analysis in $f(Q)$ gravity

Bharat Singh* and S. Surendra Singh

Department of Mathematics
National Institute of Technology, Manipur
Imphal-795004, India
Email: bharatsinghiam@gmail.com, surendra@nitmanipur.ac.in

(Received: March 12, 2025 Accepted: May 26, 2025)

Abstract

We investigated the stability conditions of $f(Q)$ gravity using a dynamical system approach, comparing the outcomes for both interacting and non-interacting dark energy models. For our analysis, we adopt a linear $f(Q)$ function of the form $f(Q) = \beta + \alpha Q$. Our analysis of the interacting model revealed two stable critical points, which we further examine through phase portraits to elucidate their physical implications. We calculate and display the values of cosmological parameters Ω_m, Ω_ϕ, ω_{Tot}, and q at every critical point, providing a comparison with observed values. Further, We also calculate the density parameters, the deceleration parameter, and the equation of state parameter and their respective graphs. The universe's fast expansion is represented by our model.

1 Introduction

Introduced in 1915, Albert Einstein's groundbreaking General Theory of Relativity transformed our comprehension of gravity and the cosmos, profoundly impacting

Keywords: $f(Q)$ gravity theory, critical point, stability analysis, cosmological interpretation.
2020 AMS Subject Classification: 83F05
***Corresponding Author**

our understanding of the Universe's fundamental nature and evolution. Indeed, general relativity is a foundational pillar of modern physics and its triumph lies in elegantly describing gravitational interactions as the curvature of spacetime, induced by the presence of mass and energy. General Relativity (GR) has withstood rigorous scrutiny through numerous experimental tests and observational evidence, spanning from the precise prediction of Mercury's orbital precession to the groundbreaking detection of gravitational waves. Despite its remarkable success, GR has its limitations, as it is unable to fully explain the entirety of the universe's phenomena, leaving room for further refinement and the development of new theories. One of the main limitations of general relativity is its inability to describe the behaviour of the universe at extremely small, quantum scales, highlighting the need for a more comprehensive theory that merges gravity with quantum mechanics. This limitation stems from the fact that general relativity is a classical field theory that neglects the fundamental principles of quantum mechanics, rendering it incompatible with the quirky and probabilistic nature of the quantum realm. Researchers have endeavoured to merge GR with quantum physics, yielding theoretical frameworks like string theory and loop quantum gravity. The latest observations from Supernova Type Ia (SNeIa) [48], Cosmic Microwave Background (CMB) radiation [46], and Baryon Acoustic Oscillations (BAO) [10] collectively provide robust evidence for the universe's accelerated expansion. Furthermore, a substantial portion of the Universe's composition is attributed to Dark Matter (DM) and Dark Energy (DE) [61], mysterious entities that lie beyond the explanatory realm of GR, necessitating the development of new theories and frameworks to account for these enigmatic phenomena. While DM and DE remain elusive, their presence can be inferred from their gravitational signatures. Notably, the latest CMBR measurements show 76% DE of the universe. The late-time acceleration of the universe is attributed to the cosmological constant, denoted by Λ, which is characterised by a negative equation of state parameter. The (EoS) parameter takes the form $\omega_\phi = \frac{p_\phi}{\rho_\phi}$ [29, 55]. The conventional cosmological model, corresponding to a cosmological constant (ΛCDM), is recovered when the equation of state (EoS) parameter ω_ϕ approaches -1, indicating a negative pressure that drives the accelerating expansion of the universe. A stiff fluid corresponds to $\omega_\phi = 1$, representing a scenario where the pressure is equal to the energy density. The matter-dominated phase is characterised by $\omega_\phi = 0$, indicating pressureless dust-like behaviour. The

radiation-dominated phase is described by $\omega_\phi = \frac{1}{3}$, where the pressure is one-third of the energy density. The universe enters the quintessence phase in both the phantom dark energy model, where $\omega_\phi < -1$, and the standard quintessence regime, where $-1 \leq \omega_\phi \leq -\frac{1}{3}$. Lastly, the cosmological constant or ΛCDM model is characterised by $\omega_\phi = -1$ [28].

However, despite the abundance of empirical data which supports the accelerated expansion of the universe, contemporary cosmology and GR are unable to reconcile with it. Cosmologists must adapt or expand GR in order to completely understand many facets of contemporary cosmology. Cosmologists need to modify GR in order to comprehend all of the many facets of contemporary cosmology. The most straightforward method of altering Einstein's theory of gravity is to substitute a function $f(R)$ for the Ricci scalar in the Einstein-Hilbert action [14]. Riemannian geometry makes it possible to formulate GR using the Levi-Civita link. Torsion and non-metricity are not used in the construction of the geometry in this framework. There are several geometric frameworks in which GR may be expressed. One such method is teleparallel gravity, in which torsion T is used to represent gravity instead of curvature R.

The symmetric teleparallel gravity framework, represented by Q, is an alternative method that defines gravitational interactions without taking torsion or curvature into account. Symmetric teleparallel gravity (ST), often known as $f(Q)$ gravity, has garnered attention recently as a contemporary and developing theory of gravity [31]. According to Weyl's geometry, the idea of Riemannian geometry serves as the basis for $f(Q)$ gravity [32]. GR is equal to $f(Q)$ gravity in flat spacetime. It has also been observed that the formulations of $f(Q)$ gravity and $f(T)$ gravity are identical.

Both $f(Q)$ and $f(T)$ gravity are governed by second-order field equations and exhibit similar dynamical behavior in the cosmic background [17]. However, notable differences emerge at the level of cosmic perturbations. While $f(Q)$ gravity theories on FLRW backgrounds often avoid such issues, $f(T)$ gravity theories generally suffer from significant coupling problems. These coupling issues are particularly evident in maximally symmetric backgrounds such as Minkowski and de Sitter spacetimes. Although such backgrounds pose major coupling challenges, these are typically less severe in $f(Q)$ gravity compared to $f(T)$ gravity. Moreover, less symmetric cosmological models—which may offer intriguing phenomenolog-

ical prospects—are unaffected by these issues. We have also demonstrated that the predictions of $f(Q)$ and $f(T)$ gravity models converge in the small-scale quasi-static limit. In contrast to $f(T)$ gravity, $f(Q)$ models propagate additional scalar degrees of freedom at larger scales. Two quintessence-based accelerating models analyzing the stability behavior of $f(Q)$ theories are investigated in [43], while [34] explores the thermodynamic properties of $f(Q)$ gravity.

This paper investigates a cosmological scenario in which the universe is homogeneous, isotropic, and composed of three main components: baryonic matter, dark energy (DE), and dark matter (DM). In this framework, baryonic matter is modeled as a perfect fluid, DE is treated as a dynamical scalar field, and DM is considered pressureless dust. The scalar field can also be equivalently described as a perfect fluid. The dynamics of baryonic matter, DM, and DE are interconnected, and they interact with one another with minimal coupling, as discussed in [39]. Cosmological models that incorporate interactions between DM, DE, and other external components have gained significant attention in recent years [23]. Interacting DE models have been proposed as potential solutions to pressing cosmological issues, such as the phantom crossing problem, the cosmic coincidence problem, and the cosmic age problem [24, 62].

In this study, we examine the implications of interacting DE within the framework of modified gravity, specifically $f(Q)$ gravity. Intense research and ongoing debate within the physics community aim to understand the nature of the interaction between DM and DE. Despite extensive efforts, the fundamental nature of both DM and DE remains unclear, making it difficult to derive a precise interaction model from first principles. Nonetheless, field-theoretical approaches often propose a reciprocal or bidirectional interaction between DM and DE, allowing for the exchange of energy and momentum between the two components. A well-designed interaction mechanism can help alleviate the cosmic coincidence problem. In the framework of $f(Q)$ gravity, we have examined the dynamical system of a scalar field [53]. Because of the intrinsic complexity and non-linearity of the underlying field equations, one of the main challenges in constructing gravity theories is the difficulty of finding analytical or numerical solutions [54]. It is difficult to directly compare Einstein's field equations with observational data because they contain nonlinear elements that are hard to solve. Alternative approaches are required to overcome this difficulty, and dynamical system analysis has become a useful tech-

nique for addressing the nonlinearities included in Einstein's field equations. It offers a framework for comprehending the qualitative behaviour of cosmological models. The stability behaviour of a particular system is investigated and numerical solutions are obtained via the use of dynamical system analysis [51]. Finding the critical points of a system of autonomous first-order ordinary differential equations—obtained by reformulating Einstein's field equations is an essential step in this method, which enables a qualitative examination of the cosmic dynamics. By computing the Jacobian matrix at each critical point and figuring out its eigenvalues, one may evaluate a model's stability [52].
We want to study the late-time acceleration in $f(Q)$ gravity using the functional form $f(Q) = \beta+\alpha Q$ in this work. The following is the structure of the manuscript: In Section 2, we present the summary of $f(Q)$ gravity theory. In Section 3, we develop some new variables and apply dynamical system analysis. In Section 4, we identify the critical points of the dynamical system and perform a stability analysis using phase plots. In Section 5, we also calculate the density parameters, the deceleration parameter, and the equation of state (EoS) parameter, along with their respective graphical representations. Lastly, Section 6 contains our conclusions.

2 Non-linear gravity theory function $f(Q)$

The metric tensor $g_{\mu\nu}$ serves as the generalized gravitational potential in the framework of differential geometry. While $Y_{\mu\nu}$ denotes parallel transport and the covariant derivative, the metric tensor $g_{\mu\nu}$ is mostly utilised for computing volumes, angles, and distances. The affine connection may be broken down into the two separate parts shown below, per [34]: the Christoffel symbol expressed as follows:

$$L^{\gamma}_{\mu\nu} + \Gamma^{\gamma}_{\mu\nu} = Y^{\gamma}_{\mu\nu}. \tag{2.1}$$

The Levi-Civita connection of the metric $g_{\mu\nu}$ appears in equation (2.1).

$$(\partial_{\mu} g_{\delta\nu} + \partial_{\nu} g_{\delta\mu} - \partial_{\delta} g_{\mu\nu})\frac{1}{2} g^{\gamma\delta} = \Gamma^{\gamma}_{\mu\nu}. \tag{2.2}$$

The distortion tensor $L^{\gamma}_{\mu\nu}$ can be expressed as:

$$(Q_{\mu\nu\sigma} + Q_{\nu\mu\sigma} - Q_{\gamma\mu\nu})\frac{1}{2}g^{\gamma\sigma} = L^{\gamma}_{\mu\nu}, \tag{2.3}$$

where $Q_{\gamma\mu\nu}$= -$\nabla_{\gamma} g_{\mu\nu}$. is the non-metricity tensor. The sum of $f(Q)$ gravity's actions is

$$\int \frac{1}{2}\, f(Q)\, \sqrt{-g}\, d^4x + \int \mathcal{L}_m\, \sqrt{-g}\, d^4x = S, \tag{2.4}$$

In accordance with [50], we define the superpotential tensor, conjugate to the non-metricity term, as follows:

$$-Q^{\gamma}_{\mu\nu} + 2Q^{\gamma}_{\mu\nu} + Q^{\gamma} g_{\mu\nu} - \widetilde{Q}^{\gamma} g_{\mu\nu} - \delta^{\gamma}_{\mu} Q_{\nu} = 4P^{\gamma}_{\mu\nu}\ . \tag{2.5}$$

The expression for the stress-energy momentum tensor is

$$-\frac{2}{\sqrt{-g}}\frac{\delta\sqrt{-g}\mathcal{L}_m}{\delta g^{\mu\nu}} = T_{\mu\nu}\ . \tag{2.6}$$

To derive the field equations, we perform a variation of the action (4) with respect to the metric tensor $g_{\mu\nu}$, following the procedure outlined in [36].

$$-T_{\mu\nu} = \frac{2}{\sqrt{-g}}\nabla_{\gamma}(\sqrt{-g} f_Q P^{\gamma}_{\mu\nu}) + \frac{1}{2} g_{\mu\nu} f + f_Q (P_{\nu\rho\sigma} Q^{\rho\sigma}_{\mu} - 2P_{\rho\sigma\mu} Q^{\rho\sigma}_{\nu}). \tag{2.7}$$

We examine a cosmological model that uses the FLRW metric in Cartesian coordinates to explain an isotropic, homogeneous, and spatially flat universe ($k = 0$):

$$ds^2 \ = a(t)^2(dx^2 + dy^2 + dz^2) + (-dt^2), \tag{2.8}$$

where t is cosmic time and $a(t)$ is the scaling factor. Similar to the spatially flat FLRW metric, the non-metricity scalar is provided by

$$6H^2 = Q\ . \tag{2.9}$$

The formula $H = \frac{\dot{a}}{a}$ With respect to time 't', the top dot represents the derivative, and the Hubble parameter is used to determine the universe's rate of expansion. The following is an expression for the stress-energy momentum tensor:

$$(\rho + p)u_{\mu}u_{\nu} + p g_{\mu\nu} = T_{\mu\nu}\ . \tag{2.10}$$

The fluid with four velocity $u_\mu u_\nu = -1$, where p denotes the isotropic pressure, ρ is the energy density, and u_μ is the fluid. The field equations for $f(Q)$ gravity using the FLRW metric are as follows [6],

$$\rho = 6f_Q H^2 - \frac{f}{2}, \tag{2.11}$$

$$-\frac{1}{2}(\rho + p) = (12f_{QQ}H^2 + f_Q)\dot{H}. \tag{2.12}$$

with $\frac{\partial^2 f}{dQ^2} = f_{QQ}$. Here we take $1 = c = 8\pi G$. The continuity equation of the stress-energy momentum tensor is $-3H(\rho + p) = \dot{\rho}$.

3 Examination of dynamical systems in $f(Q)$ gravity

The primary objective is to understand dynamical systems, especially nonlinear equations, with an emphasis on visualizing the stability of fixed or equilibrium points. Understanding cosmic behavior in the Universe necessitates a dynamical systems approach. Accurate solutions could not be determined due to the complexity of the systems [63]. The formulated as $\sigma(v) = \dot{v}$, where $\sigma : V \to V$ defines the governing function of the system. In this formulation, $\dot{v}$ denotes the time derivative, where $t \in \mathbb{R}$, and $(v_1, v_2, v_3, \ldots, v_m) = v$ is an element of the vector space V. The function $(\sigma_1(v), \sigma_2(v), \ldots, \sigma_m(v)) = \sigma(v)$ governs the evolution of the system [5]. This implies that the stability criteria were examined for m variables by solving a system of m equations. The equation $\sigma(v) = \dot{v}$ describes the time evolution of the function $v(t)$, where $\frac{dv}{dt}$ depends on v according to the function $\sigma(v)$, under given initial conditions. This condition implies that the evolution of the system is entirely determined by its current state v, where the rate of change $\dot{v}$ is governed by the function $\sigma(v)$. The equation $\sigma(v) = \dot{v}$ is referred to as an ordinary differential equation (ODE), where the rate of change of v depends on its current value v. Autonomous differential equations depend solely on the current value of the variable v and are independent of time t. A fixed point $v_0 = v$ of the system satisfies $\sigma(v_0) = 0$, meaning that if the system starts at v_0, it remains there indefinitely. This implies that v_0 is a fixed point of the system, meaning that if the system starts at v_0, it remains there indefinitely, as there is no

change in v over time. We examine small oscillations about them and analyze the behavior of the system under these perturbations. A fixed point v_0 is deemed stable if, for any small perturbation ξ, the solution $\phi(t)$ of the equation $\sigma(v) = \dot{v}$ satisfies $\xi > \|\phi(t_0) - v_0\|$ for all t, meaning that trajectories starting near v_0 remain close to it as time progresses. This implies that the fixed point v_0 is not only stable but also asymptotically stable. That is, any solution that starts sufficiently close to v_0 will not only remain close but will eventually converge to v_0 as $t \to \infty$. In contrast, a stable critical point ensures that trajectories remain within a bounded region around it but do not necessarily converge to it. An asymptotically stable critical point, on the other hand, ensures that all trajectories not only stay within a bounded region but eventually converge to the point over time. This is because, in cosmology, stable critical points typically correspond to attractor solutions, meaning that the universe naturally converges towards these states over time. Unstable critical points are characterized by nearby trajectories that initially converge but ultimately deviate and move away. Unstable critical points are characterized by trajectories that start near them but eventually diverge away. We now explore various techniques for analyzing the stability criteria of fixed points. Linear stability theory is one of the most effective approaches for examining the physical properties of cosmological models [16]. This theory linearizes the equations at key points to examine their dynamic properties. Suppose v_0 is an equilibrium point of the system $\dot{v} = \sigma(v)$. To analyze the behavior near this fixed point, we linearize the system using Taylor expansion, For each constituent $\sigma_i(v)$ of the vector field $\sigma(v)$ is expanded around v_0.

Additionally, we examine a (FRW) metric that is isotropic, homogeneous, associated with an energy density ρ_m. Model as a minimally coupled scalar field ϕ with a self-interacting potential $V(\phi)$ [4]. The energy density and pressure of the scalar field are expressed as:

$$\frac{1}{2}\dot{\phi}^2 + V(\phi) = \rho_\phi \ , \qquad \frac{1}{2}\dot{\phi}^2 - V(\phi) = p_\phi \ . \tag{3.1}$$

Finally, the recently modified Friedmann equations in $f(Q)$ gravity are expressed as:

$$\frac{1}{6f_Q}\left[\rho_\phi + \rho_m + \frac{f}{2}\right] = H^2 \ , \tag{3.2}$$

$$\dot{H} \;=\; -\frac{1}{2}\left[\frac{\rho_m+\rho_\phi+p_\phi}{12f_{QQ}H^2+f_Q}\right] = -\frac{1}{2}\left[\frac{\rho_m+\dot{\phi}^2}{2Qf_{QQ}+f_Q}\right]. \tag{3.3}$$

The energy equations are

$$0 = \dot{\rho_m} \;+3H\rho_m, \qquad 0 = \dot{\rho_\phi}+3H(1+\omega_\phi)\rho_\phi. \tag{3.4}$$

Let's examine the dynamics of a minimally coupled scalar field ϕ, which obeys the following equation:

$$0 = \frac{dV(\phi)}{d\phi} + \ddot{\phi} \;+3H\dot{\phi}. \tag{3.5}$$

Differentiation with regard to time t is shown by the overdot. This equation is widely recognized as a modified Klein-Gordon equation. Equation (3.5) cannot be solved analytically due to its complexity. To understand cosmic behavior, we must transform Equation (3.5) into an equivalent autonomous system for further analysis. The most effective approach to analyzing solution stability is introducing new variables. This transformation is particularly useful for handling exponential potentials. This method converts complex solutions into fixed points within a system of equations [57]. Therefore, we introduce dimensionless variables.

$$\frac{\dot{\phi}}{\sqrt{6}H} = x\ , \qquad \frac{\sqrt{V(\phi)}}{\sqrt{3}H} = y\ , \qquad \frac{\rho_m}{3H^2} = \Omega_m. \tag{3.6}$$

The density parameter is defined as $\Omega_m = \frac{\rho_m}{3H^2}$. By substituting the variables from Equation (3.6) into Equation (3.2), we obtain the expression for the density parameter as:

$$1 - x^2 - y^2 = \Omega_m. \tag{3.7}$$

The density parameter Ω_m satisfies the energy condition within the range $0 < \Omega_m < 1$. The pair (x, y) satisfies the equation of the circle $x^2 + y^2 = 1 - \Omega_m$ for a given Ω_m. The model is characterized by the Friedmann equation $x^2 + y^2 + \Omega_m = 1$. The values $\Omega_m = 0$ and $\Omega_m = 1$ define its boundaries. We consider $f(Q)$ in the form $f(Q) = \beta + \alpha Q$, where β and α represents the cosmological constant. The equation of state parameter ω_ϕ and the cosmological parameters associated with the scalar field are given as follows. The newly introduced dimensionless variables

lead to the expressions for the following form:

$$\omega_\phi = \frac{p_\phi}{\rho_\phi} = \frac{x^2 - y^2}{x^2 + y^2}, \quad \Omega_\phi = \frac{\rho_\phi}{3H^2} = x^2 + y^2, \tag{3.8}$$

and

$$x^2 - y^2 = \frac{x^2 - y^2}{x^2 + y^2 + \Omega_m} = \frac{p_\phi}{\rho_\phi + \rho_m} = \frac{p}{\rho} = \omega_{Tot} \text{ (by using } 1 - x^2 - y^2 = \Omega_m) \tag{3.9}$$

By utilizing the variables in Equation (3.6), the Friedmann Equations (3.2-3.3), and the given $f(Q)$ model, we obtain the following results:

$$\frac{\dot{H}}{H^2} = -\frac{3}{2\alpha}(1 + x^2 - y^2). \tag{3.10}$$

Utilizing Equation (3.10), We derive the deceleration parameter expression as follows:

$$q = -1 - \frac{\dot{H}}{H^2} = -1 + \frac{3}{2\alpha}(1 + x^2 - y^2). \tag{3.11}$$

Equation (3.10) along with the previously mentioned $f(Q)$ model can be used to express the variables in Equation (3.6) as a system of autonomous equations as follows:

$$\frac{dx}{dN} = 3x\bigg(-1 + \frac{1}{2\alpha}(1 + x^2 - y^2)\bigg) - \sqrt{\frac{3}{2}}\, y^2\lambda, \tag{3.12}$$

$$\frac{dy}{dN} = \lambda xy\sqrt{\frac{3}{2}} + \frac{3y}{2\alpha}(1 + x^2 - y^2), \tag{3.13}$$

$$\frac{d\Omega_m}{dN} = \frac{3\Omega_m}{\alpha}\,(1 - \alpha + x^2 - y^2). \tag{3.14}$$

Here, we assume $e^{\lambda\phi} = V(\phi)$, which implies that $\lambda = \frac{V'(\phi)}{V(\phi)}$. To identify the critical points, we begin by setting the system of Equations (3.12-3.14) equal to zero. Then, we study whether the key points identified in Section 4 are stable.

4 Analysis of equilibrium points and their stability

The stability characteristics of the autonomous system are analyzed at each critical point by evaluating the eigenvalues of the Jacobian matrix. The phase space is a crucial tool for understanding the behavior of dynamical systems. This study includes phase diagrams that effectively visualize the stability characteristics of the models. Identifying the critical points of the autonomous system is essential for plotting the phase graphs (3.12-3.14). To determine the critical points, we solve the system of equations defined by $x' = 0$, $y' = 0$, and $\Omega'_m = 0$. The system of Equations (3.12-3.14) yields four critical points, namely:

I. CP;A, B = $(\sqrt{2\alpha - 1}, 0, 0)$.

II. CP;C, D =$(-\frac{\alpha\lambda}{\sqrt{6}}, \pm\sqrt{1 - \frac{\alpha^2\lambda^2}{6}}, 0)$.

where $\lambda = \frac{V'}{V}$ = constant and $V' = \frac{dV}{d\phi}$ in Table 1.

Table 1 shows that the existence of fixed points C and D requires $\lambda^2 < \frac{6}{\alpha^2}$,

Table 1: Fixed points and their corresponding cosmological parameters.

Points	x	y	Ω_m	ω_ϕ	ω_{Tot}	Ω_ϕ	q
A	$\sqrt{2\alpha-1}$	0	0	1	$2\alpha-1$	$2\alpha-1$	2
B	$-\sqrt{2\alpha-1}$	0	0	1	$2\alpha-1$	$2\alpha-1$	2
C	$-\frac{\lambda\alpha}{\sqrt{6}}$	$\sqrt{1-\frac{\lambda^2\alpha^2}{6}}$	0	$\frac{\lambda^2\alpha^2}{3}-1$	$\frac{\lambda^2\alpha^2}{3}-1$	1	$-1+\frac{\lambda^2\alpha^2}{2}$
D	$-\frac{\lambda\alpha}{\sqrt{6}}$	$-\sqrt{1-\frac{\lambda^2\alpha^2}{6}}$	0	$\frac{\lambda^2\alpha^2}{3}-1$	$\frac{\lambda^2\alpha^2}{3}-1$	1	$-1+\frac{\lambda^2\alpha^2}{2}$

whereas fixed points A and B exist without any constraints. The stability analysis of the fixed points is presented in Table 1.

The characteristic values of the fixed points, presented in Table 2, are examined to determine their stability properties.

As shown in Table 2, the fixed points A and B remain hyperbolic for all values of λ. The positive eigenvalues (λ_1, λ_2, λ_3) indicate that critical point A is an unstable node, as shown in the left plot of Figure 1. However, for $\lambda < -\sqrt{6}$. This implies that λ_2 is negative, while λ_1 and λ_3 are both positive. The coexistence

Table 2: The eigenvalues corresponding to the system of Equations (3.12)-(3.14).

Points	λ_1	λ_2	λ_3	Nature
A	$6-\frac{3}{\alpha}$	$3+\lambda\sqrt{\frac{3}{2}(2\alpha-1)}$	3	unstable for $\lambda > \sqrt{6}$, saddle for $\lambda < -\sqrt{6}$
B	$6-\frac{3}{\alpha}$	$3-\lambda\sqrt{\frac{3}{2}(2\alpha-1)}$	3	saddle for $\lambda > -\sqrt{6}$, unstable for $\lambda < \sqrt{6}$
C	$\alpha\lambda^2-3$	$\frac{\alpha\lambda^2}{2}-\frac{3}{\alpha}$	$\alpha\lambda^2-3$	stable for $\lambda^2 < 3$, saddle for $3 < \lambda^2 < 6$, $\alpha = 1$
D	$\alpha\lambda^2-3$	$\frac{\alpha\lambda^2}{2}-\frac{3}{\alpha}$	$\alpha\lambda^2-3$	stable for $\lambda^2 < 3$, saddle for $3 < \lambda^2 < 6$, $\alpha = 1$

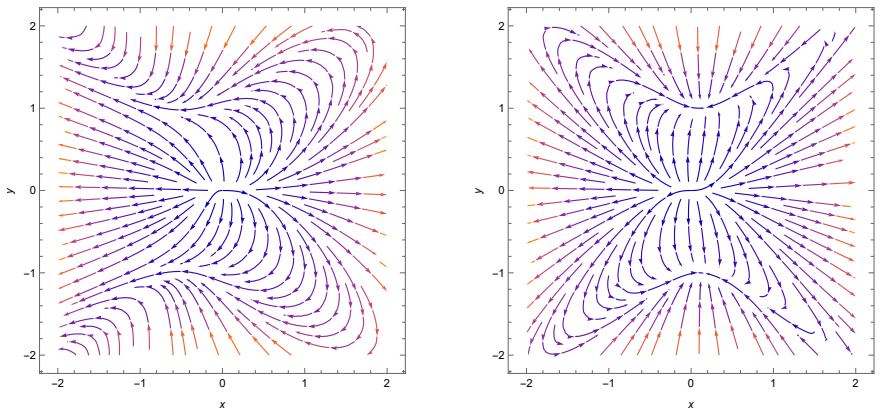

Figure 1: Phase diagrams of the System (3.12)-(3.14) with (i) $\lambda = 2.4$, $\alpha = 0.3$ (left panel), and (ii) $\lambda = -0.4$, $\alpha = 0.3$ (right panel).

of positive and negative eigenvalues characterizes point A as a saddle node, as depicted in the right plot of Figure 1. This means that two of the eigenvalues, λ_1 and λ_3, have positive values, and the third eigenvalue, λ_2, is negative. Figure 1 (left plot) depicts the unstable saddle at critical point B, This behavior arises due to the presence of both positive and negative eigenvalues. The right plot of Figure 1 shows critical point B as an unstable node, resulting from the positive nature of its eigenvalues (λ_1, λ_2, λ_3). The fact that $\Omega_m = 0$ and $\Omega_\phi = 1$ at fixed points A and B reveals a Universe in a kinetic energy-dominated phase. The values of $q = 2$

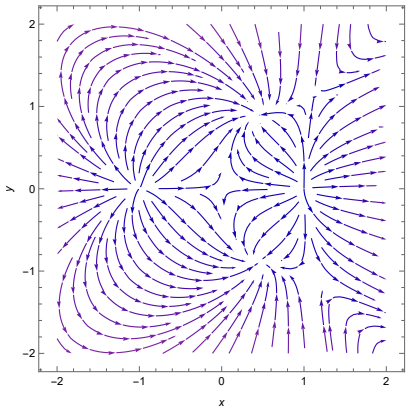

Figure 2: Phase diagram of the System (3.12)-(3.14) for $\lambda = -1.1$ and $\alpha = 0.3$.

and $\omega_{Tot} = 2\alpha - 1$ suggest that the cosmic expansion is decelerating at these sites. The divergence of trajectories from the fixed points A and B in Figure 1 suggests that these points are unstable and exhibit saddle-like behavior.

As shown in Table 1, fixed points C and D are hyperbolic for $\lambda^2 < 6$. According to Table 2, critical points C and D exhibit identical negative eigenvalues (λ_1, λ_2, λ_3) under the condition $\lambda^2 < 3$. The Figure 2 depicts critical points C and D as a stable node, due to the negativity of all eigenvalues. For the range $3 < \lambda^2 < 6$, critical points C and D have two positive eigenvalues (λ_1 and λ_3) and one negative eigenvalue (λ_2). The coexistence of positive and negative eigenvalues at these points indicates saddle point behavior, as illustrated in the Figure 2. Table 1 shows that the density parameters for sites C and D are $\Omega_m = 0$ and $\Omega_\phi = 1$, signifying a universe dominated by scalar fields. The condition $\lambda^2 < 2$ yields a deceleration parameter q that is less than zero. At critical points C and D, the universe's expansion accelerates for $\lambda^2 < 2$. Furthermore, in the ($\lambda = 0$), the total EoS parameter (ω_{Tot}) is negative and approaches -1.

The energy equations serve as the foundation for creating interacting cosmological models.

$$\mathbb{Q}^* = \dot{\rho_m} + 3H\rho_m, \tag{4.1}$$

and

$$-\mathbb{Q}^* = \dot{\rho_\phi} + 3H(1+\omega_\phi)\rho_\phi. \tag{4.2}$$

The symbol $\mathbb{Q}^*$ represents the interaction between dark energy and dark matter, implying that energy density is transferred from dark energy to dark matter. This interaction term serves as a small correction to our understanding of the universe's evolution. A positive $\mathbb{Q}$ implies a matter-dominated universe, whereas a negative $\mathbb{Q}$ indicates otherwise; at present, the universe is in a matter-dominated state. The study of large-scale structure and galaxy formation [41] is complicated by the unknown properties of DM and DE, making it difficult to constrain the interaction between them from a phenomenological perspective. The interaction term, $\mathbb{Q}^*$, is derived from the multiplication of the energy density function [64] and the Hubble parameter.

Another possible interaction between dark energy and dark matter is represented by $\mathbb{Q}^* = \eta H \rho_\phi$, with η being an extremely small, positive-definite dimensionless constant [**?**]. By leveraging Equations (3.2) and (3.3), We utilize dimensionless variables to facilitate the analysis of the dynamical system, taking into account the following key factors:

$$\frac{\dot{\phi}}{\sqrt{6}H} = x\ , \qquad \frac{\sqrt{V(\phi)}}{\sqrt{3}H} = y\ , \qquad \frac{\rho_m}{3H^2} = \Omega_m\ . \tag{4.3}$$

The autonomous system of first-order differential equations can be derived from the variables in equation (4.3) as follows:

$$\frac{dx}{dN} = -\left(\frac{\eta}{2}+3\right)x - y^2\left(\frac{\eta}{2x}+\sqrt{\frac{3}{2}}\lambda\right) + \frac{3x}{2\alpha}(1+x^2-y^2), \tag{4.4}$$

$$\frac{dy}{dN} = \sqrt{\frac{3}{2}}\lambda xy + \frac{3y}{2\alpha}(1+x^2-y^2), \tag{4.5}$$

$$\frac{d\Omega_m}{dN} = -3\Omega + \eta(x^2+y^2) + \frac{3\Omega}{\alpha}(1+x^2-y^2). \tag{4.6}$$

We assume a potential $V(\phi) = e^{\lambda\phi}$, where both the independent variable ϕ and the constant λ are present. Additionally, we introduce the logarithmic time variable $N = \log a$, which is related to the scale factor a. First, we solve equations (4.4-

4.6) by setting them to zero, which yields the critical points; subsequently, we analyze their stability.

Solving the system of equations $\frac{dx}{dN} = 0$, $\frac{dy}{dN} = 0$, and $\frac{d\Omega_m}{dN} = 0$ yields six critical points for the dynamical system represented by Equations (4.4-4.6). Table 3 summarizes the critical points obtained for the system. We evaluate the stability of the critical points by computing the Jacobian matrix from Equations (4.4-4.6) and then determining the eigenvalues associated with each point.

I. CP: A_1^*, A_2^* = $(\pm\sqrt{\frac{\alpha}{3}(n+6)-1}, 0, 0)$,

II. CP: B_1^*, B_2^* = $(-\frac{\lambda\alpha}{\sqrt{6}}, \pm\sqrt{1-\frac{\alpha^2\lambda^2}{6}}, 0)$,

III. CP: C_1^*, C_2^* = $(\pm\sqrt{1+\frac{\eta\alpha}{3}}, 0, -\frac{\eta\alpha}{3})$, in which $\lambda = \frac{V'}{V}$ = constant and $V' = \frac{dV}{d\phi}$.

Table 3: Stability points and cosmological parameter values at these points.

Points	x	y	Ω_m	ω_ϕ	ω_{Tot}	Ω_ϕ	q
A_1^*	$\sqrt{\frac{(\eta+6)}{3}\alpha-1}$	0	0	1	$\frac{(\eta+6)}{3}\alpha-1$	$\frac{(\eta+6)}{3}\alpha-1$	$2+\frac{\eta}{2}$
A_2^*	$-\sqrt{\frac{(\eta+6)}{3}\alpha-1}$	0	0	1	$\frac{(\eta+6)}{3}\alpha-1$	$\frac{(\eta+6)}{3}\alpha-1$	$2+\frac{\eta}{2}$
B_1^*	$-\frac{\lambda\alpha}{\sqrt{6}}$	$\sqrt{1-\frac{\alpha^2\lambda^2}{6}}$	0	$\frac{\lambda^2\alpha^2}{3}-1$	$\frac{\lambda^2\alpha^2}{3}-1$	1	$-1+\frac{\alpha\lambda^2}{\alpha}$
B_2^*	$-\frac{\lambda\alpha}{\sqrt{6}}$	$-\sqrt{1-\frac{\alpha^2\lambda^2}{6}}$	0	$\frac{\lambda^2\alpha^2}{3}-1$	$\frac{\lambda^2\alpha^2}{3}-1$	1	$-1+\frac{\alpha\lambda^2}{\alpha}$
C_1^*	$\sqrt{1+\frac{\alpha\eta}{3}}$	0	$-\frac{\alpha\eta}{3}$	1	$1+\frac{\eta\alpha}{3}$	$1+\frac{\eta\alpha}{3}$	$-1+\frac{\eta}{2}+\frac{3}{\alpha}$
C_2^*	$-\sqrt{1+\frac{\alpha\eta}{3}}$	0	$-\frac{\alpha\eta}{3}$	1	$1+\frac{\eta\alpha}{3}$	$1+\frac{\eta\alpha}{3}$	$-1+\frac{\eta}{2}+\frac{3}{\alpha}$

To investigate the stability of critical points in the system of equations (x, y, Ω_m), we refer to Table 4, which lists the corresponding eigenvalues.

The critical point A_1^* undergoes a loss of hyperbolicity precisely when the parameters satisfy $\lambda = -(\eta+6)/\sqrt{2\alpha(\eta+6)-6}$ and $\eta = 6$, whereas it remains hyperbolic under all other parameter combinations. Similarly, the critical point A_2^* becomes non-hyperbolic at the specific parameter values $\lambda = (\eta+6)/\sqrt{2\alpha(\eta+6)-6}$ and $\eta = 6$, while maintaining hyperbolicity for all other parameter choices. The stability properties of the critical point A_1 are contingent upon the value of the parameter λ. When $\lambda > -(\eta+6)/\sqrt{2\alpha(\eta+6)-6}$, the

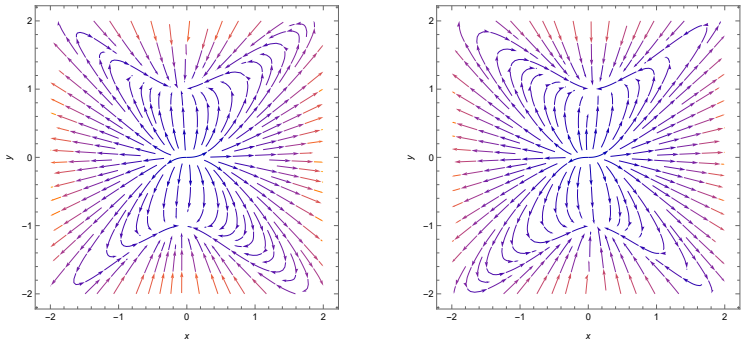

Figure 3: Phase portrait of the dynamical system (4.4)-(4.6) for (i) ($\lambda = 0.3$), ($\alpha = 0.3$, ($\eta = 0.01$ (left plot), (ii) ($\lambda = -0.3$), ($\alpha = 0.3$, ($\eta = 0.01$ (right plot).

Table 4: The eigenvalues corresponding to the system of equations (4.4-4.6).

Points	γ_1^*	γ_2^*	γ_3^*	Nature
A_1^*	$\eta+6-\frac{3}{\alpha}$	$\frac{\eta+6}{2}+\lambda\sqrt{\frac{(\eta+6)\alpha}{2}}-\frac{3}{2}$	$3+\eta$	unstable for $\lambda > -(\eta+6)/\sqrt{2\alpha(\eta+6)-6}$, saddle for $\lambda < -(\eta+6)/\sqrt{2\alpha(\eta+6)-6}$
A_2^*	$\eta+6-\frac{3}{\alpha}$	$\frac{\eta+6}{2}-\lambda\sqrt{\frac{(\eta+6)\alpha}{2}}-\frac{3}{2}$	$3+\eta$	saddle for $\lambda > (\eta+6)/\sqrt{2\alpha(\eta+6)-6}$, unstable for $\lambda < (\eta+6)/\sqrt{2\alpha(\eta+6)-6}$
B_1^*	$-\eta-3+\alpha\lambda^2+\frac{3\eta}{\alpha^2\lambda^2}$	$\frac{\alpha\lambda^2}{2}-\frac{3}{\alpha}$	$-3+\alpha\lambda^2$	stable for $\lambda^2 < 3/\alpha$ and $0 < \eta < \frac{(3-\alpha\lambda^2)\alpha^2\lambda^2}{3-\alpha^2\lambda^2}$, saddle for $\frac{3}{\alpha} < \lambda^2 < \frac{6}{\alpha^2}$ and $0 < \eta < \frac{(3-\alpha\lambda^2)\alpha^2\lambda^2}{3-\alpha^2\lambda^2}$
B_2^*	$-\eta-3+\alpha\lambda^2+\frac{3\eta}{\alpha^2\lambda^2}$	$\frac{\alpha\lambda^2}{2}-\frac{3}{\alpha}$	$\alpha\lambda^2-3$	stable for $\lambda^2 < 3/\alpha$ and $0 < \eta < \frac{(3-\alpha\lambda^2)\alpha^2\lambda^2}{3-\alpha^2\lambda^2}$, saddle for $\frac{3}{\alpha} < \lambda^2 < \frac{6}{\alpha^2}$ and $0 < \eta < \frac{(3-\alpha\lambda^2)\alpha^2\lambda^2}{3-\alpha^2\lambda^2}$
C_1^*	$\eta-3+\frac{6}{\alpha}$	$\frac{\eta}{2}+\frac{3}{\alpha}+\lambda\sqrt{\frac{\alpha\eta+3}{2}}$	$\eta-3+\frac{6}{\alpha}$	stable for $\lambda < \frac{-(\eta\alpha+6)}{\alpha\sqrt{2\alpha\eta+6}}$ and $\alpha < \frac{-6}{(\eta-3)}$, saddle for $\lambda > \frac{-(\eta\alpha+6)}{\alpha\sqrt{2\alpha\eta+6}}$ and $\alpha < \frac{-6}{(\eta-3)}$
C_2^*	$\eta-3+\frac{6}{\alpha}$	$\frac{\eta}{2}+\frac{3}{\alpha}-\lambda\sqrt{\frac{\alpha\eta+3}{2}}$	$\eta-3+\frac{6}{\alpha}$	stable for $\lambda > \frac{-(\eta\alpha+6)}{\alpha\sqrt{2\alpha\eta+6}}$ and $\alpha < \frac{-6}{(\eta-3)}$, saddle for $\lambda < \frac{-(\eta\alpha+6)}{\alpha\sqrt{2\alpha\eta+6}}$ and $\alpha < \frac{-6}{(\eta-3)}$

critical point A_1^* is characterized by three positive eigenvalues (γ_1^*, γ_2^*, and γ_3^*), rendering it an unstable node, as illustrated in the right panel of Figure 3. Conversely, when $\lambda < -(\eta+6)/\sqrt{2\alpha(\eta+6)-6}$, the critical point A_1^* exhibits a mixed stability profile, characterized by two positive eigenvalues (γ_1^* and γ_3^*) and one negative eigenvalue (γ_2^*). The coexistence of positive and negative eigenvalues signifies that the critical point A_1^* is a saddle node, with its characteristic stable and unstable manifolds depicted in Figure 3.
For values of λ less than $(\eta+6)/\sqrt{2\alpha(\eta+6)-6}$, the critical point A_2^* is characterized by three positive eigenvalues (γ_1^*, γ_2^*, and γ_3^*), indicating that it is an unstable node. The right panel of Figure 3 illustrates the unstable nature of critical point A_2^*, marked by positive eigenvalues. However, when λ surpasses the threshold $(\eta+6)/\sqrt{2\alpha(\eta+6)-6}$, the stability profile changes: while γ_1^* and γ_3^* remain positive, γ_2^* becomes negative, indicating a saddle-like behavior. The presence of both positive and negative eigenvalues confirms that the critical point A_2^* is a saddle node, as visually represented in the left panel of Figure 3. The critical points A_1^* and A_2^* are characterized by $\Omega_m = 0$ implying a universe entirely dominated by the kinetic energy of the scalar field. The phase portrait in Figure 3 reveals that the critical points A_1^* and A_2^* are unstable, as the trajectories originating from these points diverge.

The critical points B_1^* and B_2^* share the same set of hyperbolic eigenvalues. The eigenvalues γ_1^*, γ_2^*, and γ_3^* corresponding to the critical points are negative when $\lambda^2 < 3/\alpha$ and $0 < \eta < \frac{(3-\alpha\lambda^2)\alpha^2\lambda^2}{3-\alpha^2\lambda^2}$. The uniformly negative eigenvalues of critical points B_1^* and B_2^* unequivocally establish them as stable nodes, with all neighboring trajectories asymptotically converging towards these points, as visually depicted in Figure 3. The eigenvalues γ_1^* and γ_3^* are negative for $0 < \eta < 3-\lambda^2$, but γ_2^* is positive within the narrower range $0 < \eta < \frac{(3-\alpha\lambda^2)\alpha^2\lambda^2}{3-\alpha^2\lambda^2}$. The points B_1^* and B_2^* have eigenvalues with both positive and negative signs. The critical points B_1^* and B_2^* exhibit saddle point behavior, as evidenced by the mix of positive and negative eigenvalues, and illustrated in Figure 3. Table 3 indicates that the critical points B_1^* and B_2^* correspond to a universe with $\Omega_m = 0$ and $\Omega_\phi = 1$. The scalar field dominance in the universe is confirmed by the density parameters.

The critical point C_1^* exhibits non-hyperbolic behavior when $\lambda = \frac{-(\eta\alpha+6)}{\alpha\sqrt{2\alpha\eta+6}}$ and $\eta = -6$; otherwise, it remains hyperbolic. The critical point C_2^* exhibits non-

hyperbolic behavior when $\lambda = \frac{(\eta\alpha+6)}{\alpha\sqrt{2\alpha\eta+6}}$ and $\eta = -6$, but is hyperbolic otherwise. The stability of C_1^* depends on the value of λ: when $\lambda < \frac{-(\eta\alpha+6)}{\alpha\sqrt{2\alpha\eta+6}}$ and $\eta = -6$, all eigenvalues are negative, indicating stability, whereas for $\lambda > \frac{-(\eta\alpha+6)}{\alpha\sqrt{2\alpha\eta+6}}$ and $\eta = -6$, the presence of one positive eigenvalue renders the critical point unstable. The existence of eigenvalues with opposite signs confirms that the critical point C_1^* behaves as a saddle node, as illustrated in the right panel of Figure 3. For the critical point C_2^*, if $\lambda < \frac{-(\eta\alpha+6)}{\alpha\sqrt{2\alpha\eta+6}}$ and $\eta = -6$, then all eigenvalues γ_1^*, γ_2^*, and γ_3^* take negative values. This implies that C_2^* is a stable node, with all trajectories moving toward this fixed point, as shown in Figure 3. However, if $\lambda < \frac{-(\eta\alpha+6)}{\alpha\sqrt{2\alpha\eta+6}}$ and $\eta = -6$, then two eigenvalues, γ_1^* and γ_3^*, are negative, while γ_2^* is positive. The presence of both positive and negative eigenvalues indicates that C_2^* exhibits saddle node behavior, as illustrated in Figure 3.

5 Law of hybrid expansion in the $f(Q)$ gravity model

Cosmological model with exponential and power-law scale factors have been used to study the Universe's development. Existing models neglect the transition phase, assuming a constant deceleration parameter $q = -1 - \frac{\dot{H}}{H^2}$ throughout the universe's evolution. Recent findings confirm that the universe is undergoing accelerated expansion. We use a hybrid expansion law for the scale factor $a(t)$ to study the Universe's transition phase, [19, 30, 36, 44, 47, 60]

$$a_0 t^{\alpha} e^{\beta t} = a(t). \tag{5.1}$$

We derive the Hubble parameter from Equation (5.1), given the scale factor's hybrid expansion law with constants a_0, α, and β.

$$H = \frac{\dot{a}}{a} = \beta + \alpha t^{-1}. \tag{5.2}$$

From Equation (5.2), the deceleration parameter is derived as:

$$q = -1 - \frac{\dot{H}}{H^2} = -1 + \frac{\alpha}{(\beta t + \alpha)^2}. \tag{5.3}$$

In cosmology, parameters are often transformed into functions of redshift for observational relevance. The scale factor $a(t)$ and the redshift z are related by the equation $a(t) = \frac{a_0}{1+z}$, where $a_0 = 1$ denotes the current (present-day) value of the scale factor. Cosmic time and redshift are related through a derivable expression.

$$\left(\frac{\alpha W \left(\frac{\beta \left(\frac{1}{(1+z)a_1} \right)^{\frac{1}{\alpha}}}{\alpha} \right)}{\beta} \right) = t(z) \tag{5.4}$$

'W' represents the Lambert function, also referred to as the product log function. Figure 4 shows the deceleration parameter as a function of redshift for selected parameters. The deceleration parameter describes the universe's shift from deceleration to acceleration. The universe's expansion phase is determined by the deceleration parameter q: $q > 0$: deceleration, $q < 0$: acceleration, $q = 0$: marginal expansion (constant rate). Observations suggest q lies in the range $-1 \leq q \leq 0$, indicating accelerated expansion. The deceleration parameter q is plotted against redshift z in Figure 4, derived from Equations (5.3) and (5.4). The universe shifted from deceleration $(q > 0)$ at high redshifts to acceleration $(q < 0)$ at low redshifts, with $q = 0$ marking the transition point. The universe's current acceleration $q = -1$ is driven by dark energy.

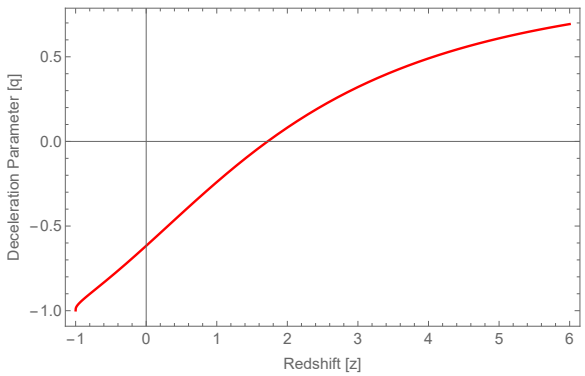

Figure 4: The evolution of the cosmic deceleration parameter q with redshift z.

The model $f(Q) = \beta + \alpha Q$ yields expressions for pressure and energy density via Friedmann Equations (2.11) and (2.12), as follows:

$$\rho = 3\alpha \left(\beta + \alpha t^{-1}\right)^2 - \frac{\beta}{2}, \tag{5.5}$$

$$p = 2\alpha^2 t^{-2} - 3\alpha \left(\beta + \alpha t^{-1}\right)^2 + \frac{\beta}{2}. \tag{5.6}$$

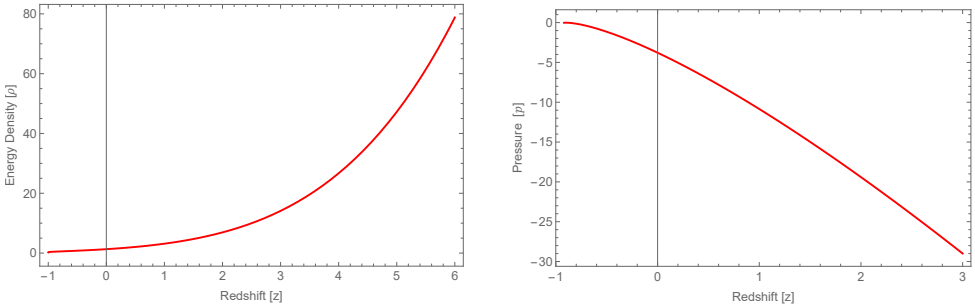

Figure 5: Pressure and energy density are evaluated by plotting them against redshift.

Figure 5 depicts the variation of energy density with redshift in the $f(Q)$ gravity model. It is clear from the figure that the energy density increases with redshift and remains positive for all values of z. Energy density begins with a large positive value and decreases to zero at present time. The pressure-redshift relationship is illustrated in Figure 5. The pressure starts high and decreases to zero in the future (as z approaches -1 is not possible, likely meant z approaches -1 in terms of evolution towards future, or more accurately as time progresses towards future, z would approach -1 is not accurate, more like pressure decreases as universe evolves forward). Recent studies confirm the universe's acceleration, driven by dark energy with positive energy density and negative pressure. The EoS parameter is derived from Equtions (5.5) and (5.6) in our model.

$$\omega_{\text{de}} = \frac{p}{\rho} = \frac{2\alpha^2 t^{-2} - 3\alpha \left(\beta + \alpha t^{-1}\right)^2 + \frac{\beta}{2}}{3\alpha \left(\beta + \alpha t^{-1}\right)^2 - \frac{\beta}{2}}. \tag{5.7}$$

Figure 6 presents the evolution of the equation of state (EoS) parameter ω as a

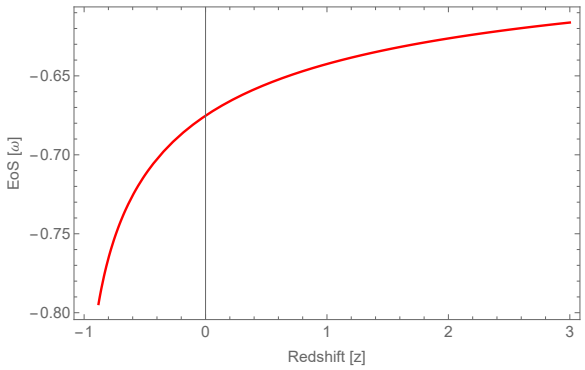

Figure 6: Evolution of the EoS parameter versus redshift curve.

function of red-shift z, showing that ω varies between $-1 \leq \omega \leq 0$. The EoS parameter ω indicates different cosmic models; $\omega = 1$; stiff fluid, $\omega < -1$; phantom model, $\omega = -1$; ΛCDM model, $-1 \leq \omega \leq -1/3$; quintessence stage. From Figure 6, ω indicates the universe is in the quintessence stage at present time $(z = 0)$ and approaches the ΛCDM model as z approaches -1 (future evolution). The model supports an accelerating universe, as shown in Figure 6. Furthermore, it is found that the present value of the EoS parameter is $\omega_0 \approx -0.88$, which is in good agreement with the Planck observational data.

6 Conclusions

We performed a dynamical system analysis of the $f(Q)$ gravity theory, a modified gravity framework that generalizes the symmetric teleparallel equivalent of general relativity. Specifically, we investigated a linear $f(Q)$ gravity model, where the gravity function takes the form: $f(Q) = \alpha Q + \beta$, here, α and β are free parameters that characterize the theory, and Q is the non-metricity scalar. A thorough stability analysis of the $f(Q)$ gravity model was undertaken, utilizing phase portraits to investigate dynamic behavior. The study compared interactive and non-interactive scenarios, shedding light on the model's stability and cosmological repercussions. In this study, we adopt an interaction term, $\mathbb{Q}^* = \eta H \rho_\phi$, that incorporates a key parameter, η, which regulates the coupling between the Hub-

ble expansion rate and dark energy density. We rewrite the differential equations obtained from the Friedmann equations using dimensionless variables (x, y, Ω_m), simplifying the mathematical framework for analyzing cosmic evolution. Solving the autonomous differential equations yielded four fixed points, which serve as the cornerstone for our subsequent examination of stability properties. We found four fixed points: A $(\sqrt{2\alpha-1}, 0, 0)$, B $(-\sqrt{2\alpha-1}, 0, 0)$, C $(-\frac{\alpha\lambda}{\sqrt{6}}, \sqrt{1-\frac{\alpha^2\lambda^2}{6}}, 0)$, and D $(-\frac{\alpha\lambda}{\sqrt{6}}, -\sqrt{1-\frac{\alpha^2\lambda^2}{6}}, 0)$. The stability analysis reveals that the fixed points C and D are stable for $\lambda^2 < 3$. Additionally, the critical points A and B describe a universe undergoing decelerated expansion, whereas C and D correspond to an accelerating universe , with the EoS parameter taking the value -1 at $\lambda = 0$. We evaluated six critical points as A_1^* $(\sqrt{\frac{\alpha}{3}(n+6)-1}, 0, 0)$, A_2^* $(-\sqrt{\frac{\alpha}{3}(n+6)-1}, 0, 0)$, B_1^* $(-\frac{\lambda\alpha}{\sqrt{6}}, \sqrt{1-\frac{\alpha^2\lambda^2}{6}}, 0)$, B_2^* $(-\frac{\alpha\lambda}{\sqrt{6}}, -\sqrt{1-\frac{\alpha^2\lambda^2}{6}}, 0)$, C_1^* $\left(\sqrt{1+\frac{\eta\alpha}{3}}, 0, -\frac{\eta\alpha}{3}\right)$ and C_2^* $\left(-\sqrt{1+\frac{\eta\alpha}{3}}, 0, -\frac{\eta\alpha}{3}\right)$ for the interaction. The stability analysis reveals that the critical points A_1^* and A_2^* correspond to unstable node and saddle node, respectively, with the parameter λ playing a crucial role in determining their stability. Critical points A_1^* and A_2^* show unstable and saddle-like dynamics, with their stability controlled by the parameter λ. The deceleration parameter $q = 2$ corresponding to points A_1^* and A_2^* reveals that the Universe undergoes a strongly decelerating expansion. Conversely, points B_1^* and B_2^* give rise to saddle and unstable solutions, whose properties are influenced by the parameters λ and η, and are characteristic of a universe undergoing accelerated expansion.

For $\lambda^2 < 2$, critical points B_1^* and B_2^* represent a quintessence-dominated era, characterized by accelerated expansion. Interestingly, when $\lambda^2 = 0$, the equation of state parameter ω_ϕ equals -1, mirroring the cosmological constant behavior of the ΛCDM model. Within the range $2 < \lambda^2 < 3$, points B_1^* and B_2^* are confirmed to be stable via local stability analysis. Furthermore, for the critical points C_1^* and C_2^*, one of the corresponding eigenvalues, γ_1^*, is expressed as $\gamma_1^* = \eta - 3 + \frac{6}{\alpha}$, providing insight into their stability properties. As a result, points C_1^* and C_2^* are non-hyperbolic, implying that their stability analysis falls beyond the realm of linear stability theory, necessitating alternative approaches to determine their stability properties. The cosmic acceleration or deceleration in the vicinity of points C_1^* and C_2^* is sensitively dependent on the parameter α, highlighting its crucial role

in shaping the dynamical evolution of the universe. The expansion of the universe accelerates for $\alpha > 1$ and decelerates for $\alpha < 1$, with the parameter α serving as a threshold for the cosmic expansion regime. Estimates of the equation of state parameter ω_ϕ from recent surveys include -1.035 (Supernovae Cosmological Project), -1.073 (WMAP+CMB), and -1.03 (Planck 2018), while the deceleration parameter q is estimated to be -1.08.

Our model uses a hybrid expansion law for the scale factor. Cosmological parameters are rewritten as functions of z. The universe's acceleration is supported by observational data. The deceleration parameter q ranges from -1 to 0. Figure 4 shows q evolving from positive to negative, approaching -1, confirming an accelerating universe. Figure 5 shows energy density is positive for all z and approaches 0 as $z \to -1$. In Figure 5, pressure is significant at higher z and approaches 0 as $z \to -1$. Positive energy density and negative pressure drive the universe's acceleration. Figure 6 illustrates the behavior of the EoS parameter ω as a function of redshift. At $z = 0$, ω lies within the quintessence regime, and as redshift decreases to $z = -1$, it approaches the value $\omega = 1$. The model's current EoS value, $\omega_0 = -0.88$, aligns with Planck observational data. We thus conclude that all observable constraints are fully satisfied by the existing model.

Acknowledgment

The author thank the referee for his careful reading of the paper and for the valuable suggestion s which greatly improved this work.

References

[1] N. Aghanim et al., *Planck 2018 results. VI. Cosmological parameters*, Astron. Astrophys. **641**, A6 (2020).

[2] U. Alam et al., *Is there Supernova Evidence for Dark Energy Metamorphosis,* Mon. Not. R. Astron. Soc., **344**(1057)(2003).

[3] R. Amanullah et al., *Spectra and Light Curves of Six Type Ia Supernovae at* $0.511 < z < 1.12$ *and the Union2 Compilation*, Astrophys. J., **716**(712)(2010).

[4] S. Arora, P. K. Sahoo, *Crossing phantom divide in $f(Q)$ gravity* Ann. Phys., **534**(2022), 2200233.

[5] E. Aydiner et al., *Late time transition of Universe and the hybrid scale factor*, Phys. Rev. D, **91**, 12 (2015a), 123002.

[6] S. Bahamonde et al., *Dynamical systems applied to cosmology: dark energy and modified gravity*, arXiv:1712.03107.

[7] B. J. Barros et al., *Testing $f(Q)$ gravity with redshift space distortions*, Phys. of Dark Universe, **30**, 100616(2020).

[8] D. Behera et al., *Nuclear symmetry energy and neutron skin thickness of ^{208}Pb using a finite-range effective interaction*, Phys. Scr. **95**(2020) 115001.

[9] G. Bengochea, R. Ferraro, *Dark torsion as the cosmic speed-up*, Phys. Rev. D **79** (2009), 124019.

[10] C. L. Bennett et al., *First Year Wilkinson Microwave Anisotropy Probe (WMAP) Observations: Preliminary Maps and Basic Results*, Astrophys. J. Suppl., **148**(2003) 175.

[11] S. Kr. Biswas, S. Chakraborty, *Interacting dark energy in $f(T)$ cosmology: A dynamical system analysis*, Int. J. Mod. Phys. D, **7**, 1550046 (2015).

[12] C. G. Boehmer, N. Tamanini, M. Wright, *Interacting quintessence from a variational approach Part II: derivative couplings*, Phys. Rev. D, **91**, 12 (2015b), 123003.

[13] D. Camarena, V. Marra, *Local determination of the Hubble constant and the deceleration parameter* Phys. Rev. Res., **2**, 013028 (2020).

[14] S. Capozziello, S. Carloni, A. Troisi, *Quintessence without scalar fields*, Astron. Astrophys., **1**(2003) 625.

[15] R. Chaubey, R. Raushan, *Qualitative study of anisotropic cosmological models with dark sector coupling*, Astrophys Space Sci., 361:215 (2017).

[16] S. del Campo, R. Herrera, D. Pavon, *Interacting models may be key to solve the cosmic coincidence problem*, arXiv:0812.2210.

[17] N. Dimakis, A. Paliathanasis, T. Christodoulakis, *Quantum Cosmology in $f(Q)$ theory*, arXiv:2108.01970v2.

[18] F. Donato, et al., *Antiprotons in cosmic rays from neutralino annihilation*, Phys. Rev. Lett. **87**(2001) 271301.

[19] V. C. Dubey et al., *Tsallis holographic dark energy in Bianchi-I Universe using hybrid expansion law with k-essence*, *J. Cosmol. Astropart. Phys.* **01**, 022 (2014).

[20] W. Fang et al., *Exact Analysis of Scaling and Dominant Attractors Beyond the Exponential Potential* Class. Quantum Grav. **26**(2009), 155005.

[21] H. Golchin, S. Jamali, E. Ebrahimi, *Interacting dark energy: Dynamical system analysis*, Int. J. Mod. Phy. D., **26** (2017), 1750098.

[22] G. Hinshaw et al., *Nine-year Wilkinson Microwave Anisotropy Probe (WMAP) Observations: Cosmological Parameter Results* Astrophys. J Suppl. Ser., **208**(19)(2013).

[23] M. Jamil, M. A. Rashid, *Constraining the coupling constant between dark energy and dark matter*, Eur. Phys. J. C., **60**(2009) 141.

[24] M. Jamil, M. Ahmad Rashid, *Interacting dark energy with inhomogeneous equation of state*, Eur. Phys. J. C., **56** (2008) 429.

[25] J. B. Jimenez, L. Heisenberg, T. Koivisto, *Coincident general relativity*, Phys. Rev. D., **98**(4)(2018), 044048.

[26] J. B. Jiménez et al., *Cosmology in $f(Q)$ geometry*, Phys. Rev. D., **101**(10)(2020), 103507.

[27] S. A. Kadam, J. L. Said, B. Mishra, *Accelerating cosmological models in $f(T, B)$ gravitational theory* Int. J. Geom. Methods Mod. Phys., DOI: 10.1142/S0219887823500834.

[28] E. Komatsu, et al., *Five-Year Wilkinson Microwave Anisotropy Probe (WMAP) Observations: Cosmological Interpretation*, Astrophys. J. Suppl., **192**(2011) 18.

[29] M. Kowalski, et al., *Improved Cosmological Constraints from New, Old and Combined Supernova Datasets*". Astrophys. J., **686**(2008) 749.

[30] M. Khurshid Alam, S. Surendra Singh, L. Anjana Devi, *Renyi Holographic dark energy and its behaviour in $f(G)$ gravity*, *Gravit. Cosmol.* **25**, 82 (2019).

[31] M. Koussour, S. H. Shekh, M. Bennai, *Anisotropic nature of space–time in $f(Q)$ gravity*, J. High Energy Astrophys., **35**(2022).

[32] M. Koussour et al., *A new parametrization of Hubble parameter in $f(Q)$ gravity*, Fortschr. Phys., **71**, 2200172 (2023).

[33] M. Koussour, S. H. Shekh, M. Bennai, *Cosmic acceleration and energy conditions in ΛCDM symmetric teleparallel $f(Q)$ gravity*, arXiv:2202.01921 (2022).

[34] M. Koussour et al., *Thermodynamical aspects of Bianchi type-I Universe in quadratic form of $f(Q)$ gravity* , arXiv:2203.03639 (2022).

[35] M. Koussour et al., *Bulk viscous fluid in extended symmetric teleparallel gravity*, Chin. J. Phys., DOI: 10.1016/j.cjph.2022.11.013.

[36] M. Koussour et al., *Bulk viscous fluid in extended symmetric teleparallel gravity*, *Chin. J. Phys.* **90**, 97 (2024), doi: 10.1016/j.cjph.2022.11.013.

[37] S. Mandal, P. K. Sahoo, J. R. L. Santos, *Energy conditions in $f(Q)$ gravity*, Phys. Rev. D., **102**(2)(2020), 024057.

[38] S. Mandal, D. Wang, P. K. Sahoo, *Cosmography in $f(Q)$ gravity*, Phys. Rev. D., **102**(12)(2020), 124029.

[39] N. Mahata, S. Chakraborty, *Dynamical system analysis for accelerating models in non-metricity $f(Q)$ gravity*, arXiv:1512.07017.

[40] N. Mahata, S. Chakraborty, *Dynamical System Analysis for a phantom model*, arXiv:1312.7644.

[41] S. K. Maurya, et al., *Relativistic massive compact stars supported by decoupled matter: Implications for mass-radius bounds*. Forstschritte der Physik, **70**, 2200061, 2022.

[42] S. C. C. Ng, N. J. Nunes, F. Rosati, *Applications of scalar attractor solutions to Cosmology*, Phys. Rev. D., **64**(2001), 083510.

[43] S. A. Narawade et al., *Dynamical system analysis for accelerating models in non-metricity $f(Q)$ gravity*, Phys. Dark Universe, **36**(2022), 101020.

[44] B. Mishra, S. K. Tripathy, *Anisotropic dark energy model with a hybrid scale factor*, *Mod. Phys. Lett. A.*, **36**, 1550175 (2015), doi: 10.1142/S0217732315501758.

[45] P. J. E. Peebles, B. Ratra, *The Cosmological Constant and Dark Energy*, Astrophys. J., **325**(1988) L17.

[46] S. Perlmutter et al., *Measurements of Omega and Lambda from 42 High-Redshift Supernovae*. Astrophys. J., **517**(1999) 565.

[47] L. Pati, B. Mishra, S. K. Tripathy, *Model parameters in the context of late time cosmic acceleration in $f(Q,T)$ gravity Phys. Scr.* **95**, 115001 (2020).

[48] A. G. Riess et al., *Observational Evidence from Supernovae for an Accelerating Universe and a Cosmological Constant*, Astron. J., **116**(1998) 1009.

[49] V. Sahni et al., *Statefinder—a new geometrical diagnostic of dark energy*, J. Exper. Theoret. Phys. Lett., **77**(5)(2003), 201.

[50] P. Saha, U. Debnath, *Anisotropic Quintessence Strange Stars in $f(T)$ Gravity with Modified Chaplygin Gas*, Adv. High Energy Phys., 2864784 (2017).

[51] A. Samaddar, S. S. Singh, *Qualitative stability analysis of cosmological parameters in $f(T,B)$ gravity*, Eur. Phys. J. C., **83**(283)(2023), https://doi.org/10.1140/epjc/s10052-023-11458-2.

[52] P. Shah, G. C. Samanta, *Stability analysis for cosmological models in $f(R)$ gravity using dynamical system analysis*, Eur. Phys. J. C., **79** (2019), 414.

[53] C. Sonia, S. S. Singh, *Dynamical systems of cosmological models for different possibilities of G and ρ_A*, Eur. Phys. J. C. **C82**, 10 (2022).

[54] S. S. Singh, C. Sonia, *Dynamical System Perspective of Cosmological Models Minimally Coupled with Scalar Field*, Adv. High Energy Phys. 2020:1-18.

[55] D. N. Spergel et al., *Wilkinson Microwave Anisotropy Probe (WMAP) Three Year Results: Implications for Cosmology*, Astrophys. J. Suppl. **170** (2007) 377.

[56] S. H. Shekh, *Models of holographic dark energy in $f(Q)$ gravity*, Phys. Dark Universe, **33**(2021), 100850.

[57] B. Wang et al., *Dark Matter and Dark Energy Interactions: Theoretical Challenges, Cosmological Implications and Observational Signatures*, arXiv:1603.08299.

[58] Y. Xu et al., *$f(Q,T)$ gravity*, Eur. Phys. J. C., **79**(8)(2019).

[59] A. K. Yadav, P. K. Sahoo, and V. Bhardwaj, *Bulk viscous Bianchi-I embedded cosmological model in $f(R,T) = f_1(R) + f_2(R)f_3(T)$ gravity*, Mod. Phys. Lett. A., 34(19)(2019), 1950145.

[60] A. K. Yadav, P. K. Sahoo, V. Bhardwaj, *Bulk Viscous Bianchi-I Embedded Cosmological Model in $f(R,T) = f_1(R) + f_2(R)f_3(T)$ Gravity Mod. Phys. Lett. A* **34**, 1950145 (2019).

[61] S. Cole et al., *The 2dF Galaxy Redshift Survey: power-spectrum analysis of the final data set and cosmological implications*. Mon. Not. R. Astron. Soc., **362**(2005) 505–534.

[62] M. Jamil, M. A. Rashid, *Interacting modified variable Chaplygin gas in a non-flat universe*, Eur. Phys. J. C., **58**(2008), 111.

[63] R. Luís, E. Rodrigues, *Discrete Dynamics in Nature and Society*, 6186354(2017).

[64] J. B. Jimenez, L. Heisenberg, T. Koivisto, *Coincident General Relativity* Phys. Rev. D., **98**(2018), 044048 .